Experimental Neurology 321 (2019) 113015

Contents lists available at ScienceDirect

Experimental Neurology

journal homepage: www.elsevier.com/locate/yexnr

Research paper

Neuronal activity and microglial activation support corticospinal tract and proprioceptive afferent sprouting in spinal circuits after a corticospinal system lesion

Yu-Qiu Jiang[a], Kristine Armada[a], John H. Martin[a,b,*]

[a] Department of Molecular, Cellular, and Basic Medical Sciences, Center for Discovery and Innovation, City University of New York School of Medicine, New York, NY, USA

[b] Neuroscience Program, Graduate Center of the City University of New York, New York, NY, USA

ARTICLE INFO

Keywords:
Spared axonal sprouting
Corticospinal tract (CST)
Proprioceptive afferents (PA)
Activity-dependence
Microglial phagocytosis

ABSTRACT

Spared corticospinal tract (CST) and proprioceptive afferent (PA) axons sprout after injury and contribute to rewiring spinal circuits, affecting motor recovery. Loss of CST connections post-injury results in corticospinal signal loss and associated reduction in spinal activity. We investigated the role of activity loss and injury on CST and PA sprouting. To understand activity-dependence after injury, we compared CST and PA sprouting after motor cortex (MCX) inactivation, produced by chronic MCX muscimol microinfusion, with sprouting after a CST lesion produced by pyramidal tract section (PTx). Activity suppression, which does not produce a lesion, is sufficient to trigger CST axon outgrowth from the active side to cross the midline and to enter the inactivated side of the spinal cord, to the same extent as PTx. Activity loss was insufficient to drive significant CST gray matter axon elongation, an effect of PTx. Activity suppression triggered presynaptic site formation, but less than PTx. Activity loss triggered PA sprouting, as PTx. To understand injury-dependent sprouting further, we blocked microglial activation and associated inflammation after PTX by chronic minocycline administration after PTx. Minocycline inhibited myelin debris phagocytosis contralateral to PTx and abolished CST axon elongation, formation of presynaptic sites, and PA sprouting, but not CST axon outgrowth from the active side to cross the midline. Our findings suggest sprouting after injury has a strong activity dependence and that microglial activation after injury supports axonal elongation and presynaptic site formation. Combining spinal activity support and inflammation control is potentially more effective in promoting functional restoration than either alone.

1. Introduction

Brain and spinal cord injury typically disrupt multiple descending motor pathways leading to motor impairments and paralysis. Motor deficits are primarily rooted in the loss of cortical control due to disconnection of corticospinal tract (CST) axons (Brooks and Stoney Jr., 1971; Martin, 2005; Lemon, 2008), which show very limited regeneration capacity (Silver et al., 2014), within spinal circuits. Thus, the post-injury prognosis–for both the likelihood of motor recovery as well as the development of further impairment, such as spasticity—is largely determined by reorganization of spared motor pathways and spinal motor circuits (Bareyre et al., 2004). Selective lesion of CST axons in the medullary pyramid has been widely used for studying the rewiring of spinal motor circuits due to the functional significance of this pathway (Filipp et al., 2019). After CST lesion, spinal motor circuits reorganize, a process that includes: degeneration of CST axons; loss of a class of target interneuron (Jiang et al., 2013; Jiang et al., 2016; Jiang et al., 2018); and a gain of new axonal projections from spared pathways, including the ipsilateral CST and proprioceptive afferent fibers (Z'Graggen et al., 1998; Bareyre et al., 2004; Brus-Ramer et al., 2007; Tan et al., 2012; Williams et al., 2017).

While spared axons typically show injury-dependent sprouting (Schwab, 2002; Brus-Ramer et al., 2007), they are also sensitive to activity-based manipulations (Martin and Lee, 1999; Brus-Ramer et al., 2007; Jiang et al., 2016). Importantly, it is difficult to distinguish the contributions of injury and activity loss to post-injury circuit remodeling because the loss of connections due to injury produces an immediate loss of CST motor control signals and, consequently, spinal cord activity. CST sprouting after injury depends on similar growth-related signaling pathways (Lang et al., 2013; Lee et al., 2014) as

* Corresponding author at: Department of Molecular, Cellular, and Biomedical Sciences, City University of New York School of Medicine & Center for Discovery and Innovation, 160 Convent Avenue, New York, NY 10031, USA.
E-mail address: jmartin@ccny.cuny.edu (J.H. Martin).

https://doi.org/10.1016/j.expneurol.2019.113015
Received 6 January 2019; Received in revised form 12 May 2019; Accepted 17 July 2019
Available online 18 July 2019
0014-4886/

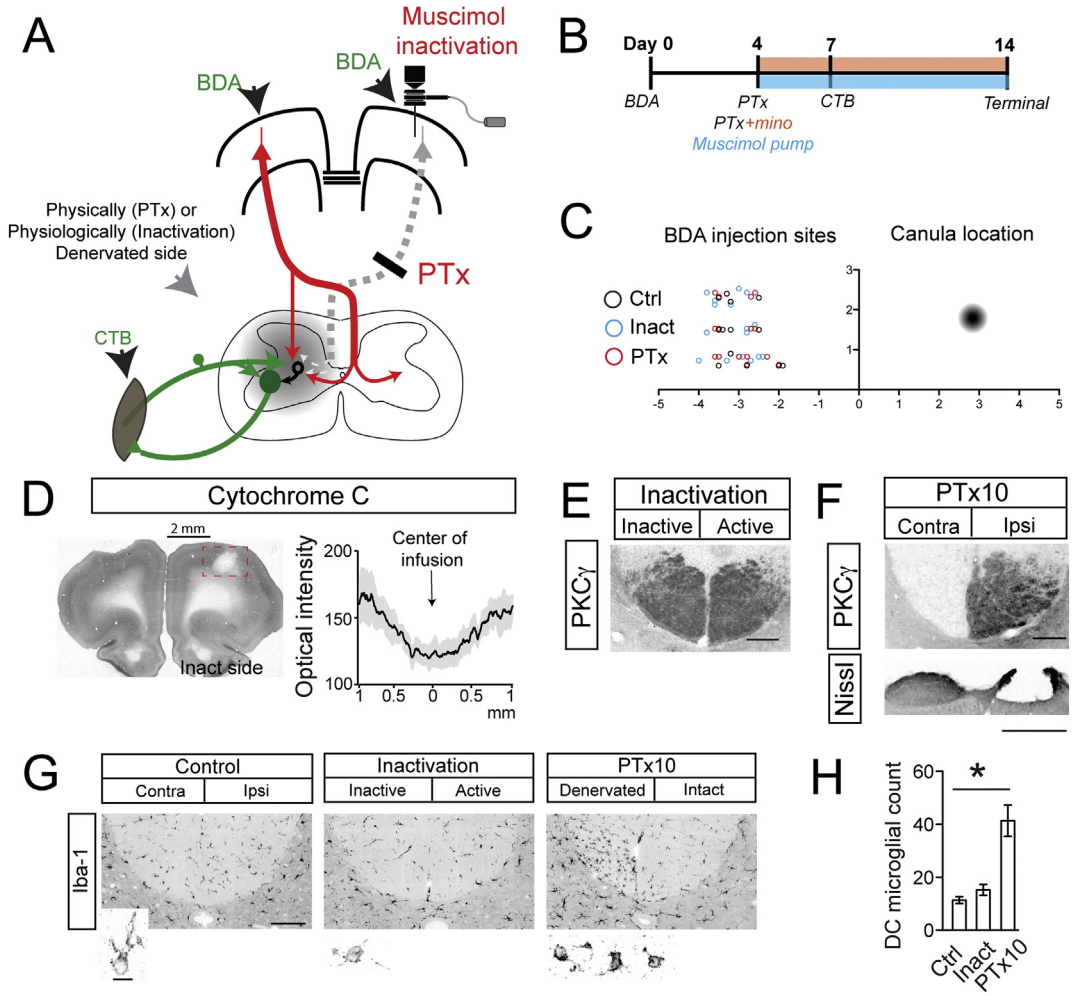

Fig. 1. Experimental design and verification. A. Schematic illustration of experimental design. Gray matter shading on the left side indicates denervated/inactivated side. B. Time line of individual procedures. C. Summary of the BDA injection locations in all groups on the left side, and muscimol infusion cannula site on right side. D. Representative cytochrome C histochemical staining (left; 40 μm section) and plot profile analysis of cytochrome C optical intensity in the infusion area (right; $N = 4$ rats) reveals reduced metabolic activity in infused motor cortex. E. PKCγ staining reveals no CST axonal damage in the inactivated dorsal column. F. Unilateral PTx causes complete loss of PKCγ staining in the injured dorsal column (top). Nissl staining of lesion site at medulla reveals that the lesion is limited to pyramidal tract (bottom). G. Iba-1 staining shows that no obvious microglial activation was induced in the dorsal column after 10 days of MCX inactivation compared to control; PTx induces dense microglial cell staining in the injured dorsal column. Insets (below) are higher magnification images of Iba-1 positive microglial cells in each group. H. Quantification of Iba-1 + microglial cells in the injured dorsal column of the spinal cord from all groups. Cortical inactivation did not produce a significant increase in the number of microglial cells in the injured DC as did PTx. Kruskal-Wallis test, $p = .0258$; Dunn's multiple comparison test, $^*p < .05$. Scale: 100 μm in E, F, and dorsal column images in G. 10 μm for insets in G.

activity-dependent sprouting (Zareen et al., 2018). We thus hypothesize that the immediate loss of activity of spinal circuits that have been partially denervated after pyramidal tract lesion (PTx) is an important factor governing sprouting of axons spared after injury.

In addition to intrinsic activity-dependent mechanisms, the capacity for CST axon outgrowth after injury is also modulated by extrinsic factors (Tedeschi and Bradke, 2017). Particularly, axonal injury and the subsequent Wallerian degeneration induce inflammatory responses (Kumar and Loane, 2012; Spejo and Moon, 2018). Although injury-induced neuroinflammation show both beneficial and harmful effects on post-injury repair (Popovich and Longbrake, 2008), spared axonal sprouting has been mostly shown to be promoted by inflammation at or near an injury site, which is most likely contributed by infiltrated peripheral macrophages and immune cells (Guth et al., 1994; Vallieres et al., 2006; Chen et al., 2008; Popovich et al., 2012; Torres-Espin et al., 2018). Macrophages, in particular, were found to support regeneration and functional recovery via phagocytosis of dead tissues and trophic support (Lazarov-Spiegler et al., 1996). However, sprouting is not limited to the location near the injury, but also is present at sites distant from injury (Chen et al., 2008; Tan et al., 2012; Bachmann et al., 2014; Lindau et al., 2014), where neuroinflammation primarily evolves due to the presence of activated innate CNS immune cells, the microglia (George and Griffin, 1994; Popovich et al., 1997). We thus further hypothesize that after PTx, sprouting of spared axons in the cervical spinal cord requires adequate post-injury inflammation, especially microglial activation and clearance of myelin debris.

To explore the role of activity loss in regulating spared CST and proprioceptive afferent sprouting, we compared the effects of unilateral PTx and MCX inactivation in adult rats. PTx eliminates the CST from one hemisphere and this, in turn, triggers CST sprouting from the MCX in the other hemisphere (Brus-Ramer et al., 2007), as well as sprouting of proprioceptive afferents in the spinal cord (Tan et al., 2012). We use MCX inactivation to test if the loss of activity, like the loss of CST axons and their connections after PTx, is a suitable trigger for the active CST axons from the other hemisphere and cervical proprioceptive axon to sprout. To address injury-induced inflammation at remote locations, especially microglial involvement in axonal sprouting, we blocked inflammation (including microglial activation) after PTx using

minocycline, a relatively specific and highly effective inhibitor of microglial activation and inflammation (Garrido-Mesa et al., 2013; Shultz and Zhong, 2017). By comparing CST and PA sprouting following PTx alone and PTx plus minocycline, we intend to identify a role for inflammatory responses, and the likely clearance of myelin debris after injury by activated microglia, in promoting sprouting.

We found that MCX inactivation increased the formation of CST presynaptic sites and PA sprouting, whereas PTx additionally produced CST axon elongation, in the inactivated/denervated ipsilateral gray matter and that this injury-dependent axon sprouting response was blocked by minocycline. Our findings suggest that an important component of spared CST and PA sprouting after PTx is due to the loss of activity that occurs as a consequence of the injury. That injury-induced remote inflammatory responses, represented by microglial activation, are necessary for sprouting to occur underscores the myriad factors that organize neural remodeling after a remote injury.

2. Material and methods

2.1. Animals

Experiments were performed in accordance with the National Institutes of Health Guidelines for the Care and Use of Laboratory Animals. All animal protocols were approved by the City College and the City University of NY Institutional Animal Care and Use Committees. Adult male Sprague Dawley rats (250-300 g) were housed under a 12 h light/dark cycle in a pathogen-free area with water and food provided ad libitum. All surgeries were performed under general anesthesia (70 mg/kg ketamine, 6 mg/kg xylazine, i.p.) and aseptic condition.

2.2. Experimental and surgery procedure

A schematic of our experimental plan is shown in Fig. 1A. The CST was anterogradely labeled with biotinylated dextran amine (BDA) injected into the forelimb representation of MCX. Muscle proprioceptive afferents (PA) were labeled transganglionically using cholera toxin B subunit (CTB) injected into the extensor carpi radialis (ECR) muscle, which also retrogradely labels ECR motoneurons. Surgeries were performed according to the time line shown in Fig. 1B.

2.2.1. Chronic M1 muscimol infusion

To block the activity of motor cortex chronically, the $GABA_a$ receptor agonist Muscimol (10 mM in normal saline, Sigma) was continuously infused for 10 days using an implanted osmotic minipump (Alzet, model 2002, 0.5 µl/h) (Martin and Ghez, 1999). The infusion canula was centered in right M1 forelimb representation (AP: 1.8 mm, ML: 3 mm as shown in Fig. 1C, right) (Brus-Ramer et al., 2009; Jiang et al., 2013), and at a depth of 1.5 mm below the pial surface. Depression of cortical neuronal activity was confirmed using a metabolic marker, as loss of Cytochrome C staining (Wong-Riley, 1989), in each animal ($n = 4$; Fig. 1D left), which is analyzed using plot profile function in ImageJ and summarized in Fig. 1D right.

2.2.2. Pyramidal tract lesion (PTx)

Animals were anesthetized (ketamine and xylazine: 70/6 mg/kg, i.p.) and a small craniotomy was made in the ventral surface of occipital bone to expose the right pyramidal tract at the caudal medullary level. An iridectomy scissor was lowered to a depth of 1.2 mm below the ventral medullary surface directly adjacent to the basilar artery and the entire right pyramid was transected as described before (Brus-Ramer et al., 2007) (Fig. 1A). We verified the completeness of pyramidal tract lesion in each animal by two ways: absence of pyramidal tracts with Nissl staining in medulla (Fig. 1F lower), and complete loss of PKCγ staining in the cervical dorsal column contralateral to the PTx (see Fig. 1F, upper). Medullary Nissl staining also indicates no further injury to pathways adjacent to pyramidal tracts.

2.2.3. Anterograde labeling of MCX corticospinal axons

Seven injections of BDA (10%, 300 nl/injection site, Invitrogen) were made into forelimb motor cortex, the coordinates of seven sites are (AP, ML in mm): (1.0, 2.0), (1.0, 3.0), (1.0, 4.0), (1.8, 2.5), (1.8, 3.5), (2.5, 2.5), (2.5, 3.5). The exact location may be slightly shifted when blood vessels were encountered (Fig. 1C, left). Injections were made 1.5 mm below the pia surface. The injections sites distribute evenly within forelimb motor cortex and are consistent between control, inactivation and PTx animals. To study spared CS axonal sprouting, BDA was injected to either unlesioned MCX in PTx animals, or the active MCX in inactivation animals. To study the phagocytosis of the inactivated CST, BDA was injected to muscimol infused MCX in inactivation animals. We summarized the injection sites in Fig. 1C.

2.2.4. Muscle afferents tracing

CTB (1%; 10 µl, List Biologicals) was injected into the extensor carpi radialis muscle (ECR) at the side with either CS denervation or MCX inactivation using a Hamilton syringe (Jiang et al., 2016).

2.2.5. Systemic minocycline administration

Minocycline hydrochloride was administered to PTx rats daily for 10 days ($n = 4$; Sigma. 45 mg/kg, pH adjusted to 7.4, i.p.) to achieve a maximal inhibitory effect (Jiang et al., 2018), and the first dose was given immediately after PTx, as described previously (Jiang et al., 2018).

2.3. Tissue preparation and staining

Animals were deeply anesthetized and perfused with saline followed by 4% paraformaldehyde. Frozen brain and spinal cord tissues were cut transversely at 40 µm thickness using a sliding microtome. For Cytochrome oxidase histochemical staining, brain sections were incubated for 2–6 h at 37 °C in 0.1 M phosphate buffer containing 4% sucrose, 0.05% DAB, and 0.03% cytochrome C (Sigma type III). For CST analysis, BDA was visualized with 1% avidin– biotin complex reagent (Vector Laboratories), and followed by the chromogen diaminobenzidine (DAB; Sigma) or streptavidin conjugated to FITC or Cy3. The following primary antibodies were used: goat anti- CTB (1: 1000, List Biologicals), guinea pig anti- VGLUT1 (1:1000, Millipore), rabbit anti-Iba-1 (1:1000, Wako), mouse anti- myelin basic protein (1:1000, MBP). FITC, Cy3 or Cy5 conjugated donkey anti-goat, donkey anti-guinea pig, donkey anti-mouse, donkey anti-rabbit secondary antibodies were used subsequently according to the combination of co-labeling. Finally, Sections were digitally imaged using Zeiss LSM 880 confocal microscope.

2.4. Image analysis of cervical 6–8 spinal cord segments

2.4.1. Quantification of midline crossing axons

BDA-labeled uninjured or active CST axons located within a 25 µm wide rectangle near the border of Laminae VII and X were counted to obtain an estimate of the number of midline crossing axons, as shown in Fig. 3A (middle panel, red rectangles) (Brus-Ramer et al., 2007). For each animal, 10–15 sections were quantitatively analyzed.

2.4.2. Corticospinal axon length estimation

Uninjured or active CST axons were manually-traced and axon varicosities (approximately $\geq 3\times$ the stem axon diameter) were marked using Neurolucida (MBF Science). The traced axon length and varicosity numbers were obtained using Neurolucida Explorer. The estimation of axon length was corrected for the variability in tracing between animals using the average number of BDA-labeled axons in the dorsal CST estimated using the Optical Fractionator program in Stereo Investigator (MBF Science). For this analysis, 4–5 sections were selected

for quantitative measurements in each animal.

2.4.3. Proprioceptive afferent terminal density analysis

High-resolution tiled images of CTB-labeled spinal cord sections were captured using a Zeiss 880 confocal microscope at 20× with an optical thickness of 1 μm. Because we were interested in changes within the gray matter only, the white matter areas of the spinal cord were digitally removed before analyses. All images underwent selective threshold adjustments using equivalent contrast/brightness levels to highlight only CTB-labeled fibers, which reduced noise variations between sections and animals (Photoshop; Adobe); this has been described in our previous study (Tan et al., 2012). The mediolateral distribution of CTB-positive terminals in the deep dorsal horn/intermediate zone (Fig. 5 B-E, rectangle) was analyzed on the thresholded images using the Plot Profile function in ImageJ. And the area under medial and lateral parts of the distribution curves were calculated in using the program Prism 5. For each animal, 10–15 sections were analyzed.

2.4.4. Density heatmaps

Axon tracing data or processed CTB images from individual sections were corrected for orientation and aligned with one another according to fiduciary marks, and then were exported and quantified using custom programs written in Matlab (MathWorks). Output files of individual sections of the spinal gray matter were divided into 40 μm by 40 μm square regions of interest (ROIs). Axon length, varicosity numbers, and CTB-positive terminal densities are represented according to a color scale, from the lowest density (blue) to the highest (red). Areas without labeling are colored black. To compare the distribution of uninjured or active CST varicosities and PA terminals, we warped the heatmaps in photoshop to match the contour within MCX inactivation or PTx groups.

2.4.5. Dorsal column microglia cells count

Microglial cells were visualized using Iba-1 staining. We obtained 40× confocal z-stack images within dorsal column as the area of interest (ROI; 212.5 × 212.5 μm). Only Iba-1 positive cells with a clear soma and processes were counted as shown in Fig. 1G insets. For each animal, 4 sections were analyzed.

2.4.6. Quantification of microglial engulfment of myelin or CST axonal debris

Intensity of myelin basic protein (MBP) or BDA clusters within individual microglia were obtained using ImageJ. Images were thresholded using consistent values, and only clusters with ≥3 pixels were circled for optical intensity analysis, similar to our previous study (Jiang et al., 2018). For clusters occupying several optical slices, we analyzed the slice containing the largest cluster area. If multiple clusters appeared in one microglial cell, the intensity of all clusters was summed to represent the value of the corresponding microglial cell. Images were taken from 3 animals in each group with a focus on the medial intermediate zone, which is where contralateral CS axons are densest (Jiang et al., 2016). For this analysis, 8 sections were randomly chosen from each animal, and 25–70 microglial cells were analyzed from each animal, the numbers of cells varied due to the distinct inflammatory condition with or without injury. As a result, the total numbers of microglia cells that were analyzed ranged from 100 to 200 for each group.

Statistics. Statistical analyses were performed using Prism 5 (Graph Pad Prism 5). For data not normally distributed, the Mann-Whitney test was used to compare two groups. The Kruskal-Wallis test was used to compare more than two groups, which was followed by Dunne's Multiple comparison test. Data that were verified to be normally distributed were compared with a One-way ANOVA followed by the Tukey Multiple comparison test. Cumulative curves were compared using the Kolmogorov-Smirnov (K−S test).

3. Results

3.1. Corticospinal inactivation did not lesion the CST

We used MCX inactivation to identify activity-dependent sprouting of CST and PA axons in adult rats. Using cytochrome C staining, we confirmed successful activity depression in motor cortex after chronic muscimol infusion in all 4 animals (Fig. 1D). To verify that inactivation did not lesion CST axons, we first verified the expression of the CST marker PKCγ in the dorsal column. The inactivated CST shows the same level of PKCγ staining as the active (ipsilateral) dorsal column (Fig. 1E). This contrasts with the complete loss of PKCγ-immunoreactivity in the lesioned dorsal column after PTx (Fig. 1F upper). We next compared the expression of microglial cells in the inactivated and active sides of the dorsal column. The proliferation of microglial cells is a sensitive indicator of inflammation associated with axonal injury in the brain and spinal cord (Riva-Depaty et al., 1994; Greenhalgh and David, 2014). We detected symmetric and small numbers of Iba-1+ microglial cells in both sides of the dorsal column after unilateral cortical inactivation (Fig. 1G). Quantification (Fig. 1H, inact) revealed no significant increase in dorsal column microglial cell numbers compared to control animals. This contrasts with a strong increase 10 days after PTx (Fig. 1H, PTx10) (ctrl: 11.3 ± 1.3, inact: 15.2 ± 2.0, PTx10: 41.3 ± 6.0; Kruskal-Wallis test, $p = .0258$; Dunn's multiple comparison test, $^{*}p < .05$). These findings indicate that inactivation did not induce an injury-associated inflammatory response in the dorsal columns after cortical muscimol infusion, and that there was no detectable loss of or injury to descending CST axons. Thus, different from physical denervation by PTx, cortical inactivation introduces a physiological denervation in the contralateral spinal cord.

3.2. Corticospinal inactivation and PTX increased microglial phagocytosis on the affected side of the spinal gray matter

Microglia is the major innate immune cell class in the brain and spinal cord. Using its phagocytosis function, microglia participate in maintaining the structural and functional homeostasis of the central nervous systems, such as normal myelin turnover (Ando et al., 2003; Yeung et al., 2014; Safaiyan et al., 2016), and activity –dependent synaptic plasticity (Nimmerjahn et al., 2005; Tremblay et al., 2010; Parkhurst et al., 2013). This phagocytosis is significantly up-regulated after injury, as part of injury-associated inflammatory responses, in order to engulf damaged neuronal and axonal debris (Riva-Depaty et al., 1994; Greenhalgh and David, 2014; Jiang et al., 2018). Indeed, as shown in the set of representative images (Fig. 2A), we detected myelin basic protein clusters (MBP, arrowhead) within microglial cells in the gray matter of denervated spinal cord in the PTx animals, consistent with phagocytosis of myelin debris. We measured the presence of myelin in microglial cells in the normal and PTx-denervated spinal gray matter of all groups and quantified the optical intensity of microglial MBP clusters (Fig. 2B). The mean intensity of microglial MBP clusters increased significantly 3 days after PTx, with a slight decline at 10 days (ctrl: 65.5 ± 5.0, PTx3: 145.9 ± 11.8, PTx10: 97.5 ± 8.9; One Way ANOVA, $p < .0001$; Tukey's multiple comparison test, $^{**}p < .01$, $^{*}p < .05$). The increased microglial MBP level in the denervated spinal cord reflects microglial phagocytosis of myelin, which could be due to Wallerian degeneration after PTx. Chronic application of minocycline, an inhibitor of microglial cells, completely blocked the increase in microglial phagocytosis of myelin (Fig. 2B, PTx10 + mino: 56.8 ± 5.1; Tukey's multiple comparison test, $^{*}p < .05$). This is consistent with our previous finding that minocycline was effective in completely blocking the phagocytic actions of microglia on premotor cholinergic interneurons in the spinal gray matter (Jiang et al., 2018).

Despite no significant lesion-associated microglial proliferation in the dorsal column after cortical inactivation, compared with PTx (Fig. 1G), we recently showed that MCX inactivation drives a higher

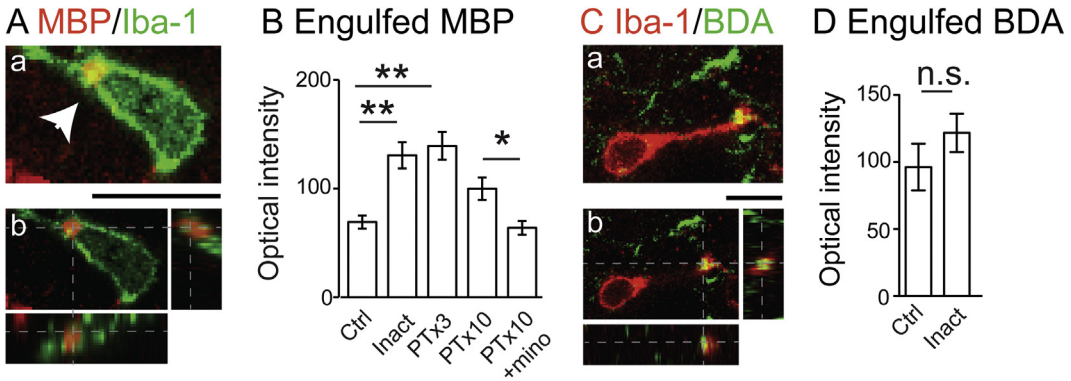

Fig. 2. Both MCX inactivation and PTx increase microglial phagocytosis of myelin, which is blocked by minocycline treatment. A. Representative images showing myelin debris (MBP, red, arrow head) within a microglia cell (Iba-1, green), indicating microglial phagocytosis of myelin debris. Part a is projection of the z- stack image; b shows a single 1 μm optical plane image. X and Y views are also shown. B. Optical intensity of microglia-engulfed MBP clusters. One Way ANOVA, $p < .001$; Tukey's multiple comparison test, $^{**}p < .01$, $^{*}p < .05$. C. Representative images showing inactivated CST axonal debris (BDA, green) within microglia (Iba-1, red), indicating phagocytosis of corticospinal axon debris. Part a is a projection of the z- stack image; b shows a single 1 μm optical plane image. X and Y views are also shown. D. Optical intensity of microglia-engulfed inactivated CS axonal debris. Mann Whitney test, $p = .1012$. Scale in A and C: 10 μm. (For interpretation of the references to colour in this figure legend, the reader is referred to the web version of this article.)

number of activated microglial cells (i.e., showing the phagocytic phenotype) in the spinal gray matter (Jiang et al., 2018). Consistently, we also found significantly more microglial MBP signal after MCX inactivation compared to that of controls (Inact: 130.7 ± 12.1, Tukey's multiple comparison test, $^{**}p < .01$). Moreover, it is not different from the value of the two PTx groups. These findings imply that cortical inactivation is sufficient to drive microglial phagocytosis of myelin debris within the gray matter as after PTx. We next took advantage that the inactivated CST axons remain intact and continue to be labeled by BDA to determine if CST axonal components (BDA) was also engulfed by activated microglia (Fig. 2 C). We were able to detect BDA-positive puncta in microglial cells (Fig. 2C), reflecting normal surveillance by microglial cells (Nimmerjahn et al., 2005). However, the quantification of engulfed BDA puncta in microglia showed no significant increase in the inactivated spinal cord compared to that of the controls (Fig. 2D. ctrl: 96.3 ± 17.5, inact: 121.8 ± 14.3; Mann Whitney test, $p = .1012$). This shows that despite increased clearance of myelin debris, inactivated CS axons remains stable after inactivation. Thus, we conclude that MCX inactivation primarily caused an activity-dependent demyelination in spinal gray matter, without evidence for axon loss.

3.3. CST axons in all groups were equally potentiated to cross the midline but differently elongate in the gray matter

The major source of ipsilateral CST axons is the intact CST axons that re-cross the midline within lamina X of the spinal cord (midline crossing, Fig. 3A schematic image on left). In the representative images in Fig. 3A (enlarged in middle panel), few midline crossing axons were detected in the control spinal cord. Many of the intact CST axons can be seen to make hairpin-like U turns when they approach the midline (arrow). In contrast, axons crossing the midline are frequently detected after inactivation, PTx10, and PTx10 with minocycline treatment. Quantification showed a significant and nearly 3-fold increase in the numbers of midline-crossing axons within a 40-μm section in inactivation and PTx10 animals, with or without minocycline treatment, compared with controls (Fig. 3B. ctrl: 1.2 ± 0.3, inact: 3.4 ± 0.3, PTx10: 3.5 ± 0.2, PTx10 + mino: 3.2 ± 0.2; Kruskal-Wallis test, $P < .0001$; Dunn's multiple comparison test: $^{***}P < .0001$). Considering that the length of the cervical enlargement is approximately 1 cm, containing ~250 40-μm sections, the total increase in crossing axon numbers can reach nearly 1000 along the cervical enlargement. These findings show that cortical inactivation is sufficient to promote sprouting of spared CST axons to the same extent as after PTx, which induces activity loss immediately after lesion as well as a complete loss of CST projections from the lesioned side. Inhibition of PTx-induced inflammation by minocycline did not interfere with this sprouting potential.

With newly sprouted axons entering the denervated or inactivated spinal cord gray matter, axonal elongation is required to achieve a denser and more extensive termination, which is particularly remarkable only in the PTx10 spinal cord (Fig. 3A; heatmaps). To quantify axon elongation, we measured the length of individually traced axons in the four groups, and plotted the data as frequency distribution curves, which were then fitted to Gaussian distributions (Fig. 3C). The inactivated group was not different from controls (Fig. 3C, black and blue curves, K–S test, $p = .5307$). The PTx10 group (red curve) showed a significant axon length shift to the right; a lower percentage of short axons (double red arrows), and a larger percentage of longer axons (single red arrow) compared with controls (K–S test, $p < .0001$). Minocycline treatment (green curve) led to the opposite pattern, with more shorter axons (double green arrows) and fewer longer axons (single green arrow) compared with controls (K–S test, $p < .0001$) and with the PTx10 group (K–S test, $p < .0001$). Similarly, the mean length of individual axons showed a significant increase in the PTx10 group, whereas cortical inactivation did not trigger a change compared with controls. Minocycline treatment blocked the axonal elongation in PTx animals, with a mean length that is even shorter than that of the control animals (Fig. 3D. ctrl: 51.2 ± 1.5, inact: 50.0 ± 1.2, PTx10: 59.1 ± 1.9, PTx10 + mino: 45.5 ± 1.4; Kruskal-Wallis test, $P < .0001$; Dunn's multiple comparison test: $^{***}P < .0001$, $^{**}P < .01$). As a result of CST axon elongation after PTx, but not MCX inactivation, total CST axon length in affected spinal cord (Fig. 3E) showed: no significant change immediately after 10 days of MCX inactivation, but approximately a 107% increase 10 days after PTx, and minocycline completely abolished the increase after PTx ($x10^3$ μm, Ctrl: 5.18 ± 0.34, Inact: 6.19 ± 0.42, PTx10: 10.74 ± 0.10, PTx10 + mino: 4.65 ± 0.37; Kruskal-Wallis test, $p = .0001$, Dunn's Multiple Comparison test, $^{***}p < .001$, $^{**}p < .001$). Again, the averaged changes in a 40- μm section reflects a substantial amount sprouting along the entire cervical enlargement. This is also shown in the heatmaps as much broader and denser terminations in the PTx10 group, but not in inactivation or minocycline groups, comparing with controls (Fig. 3A, lower panel). Together these findings indicate that suppression of neuronal activity is sufficiently strong to provoke active CST axons to cross the midline to enter the denervated spinal cord to the same extent as after PTx. Injury-induced inflammation, which is represented by activation of phagocytic microglia, and robust after PTx, was not involved in determining the capacity for midline axonal

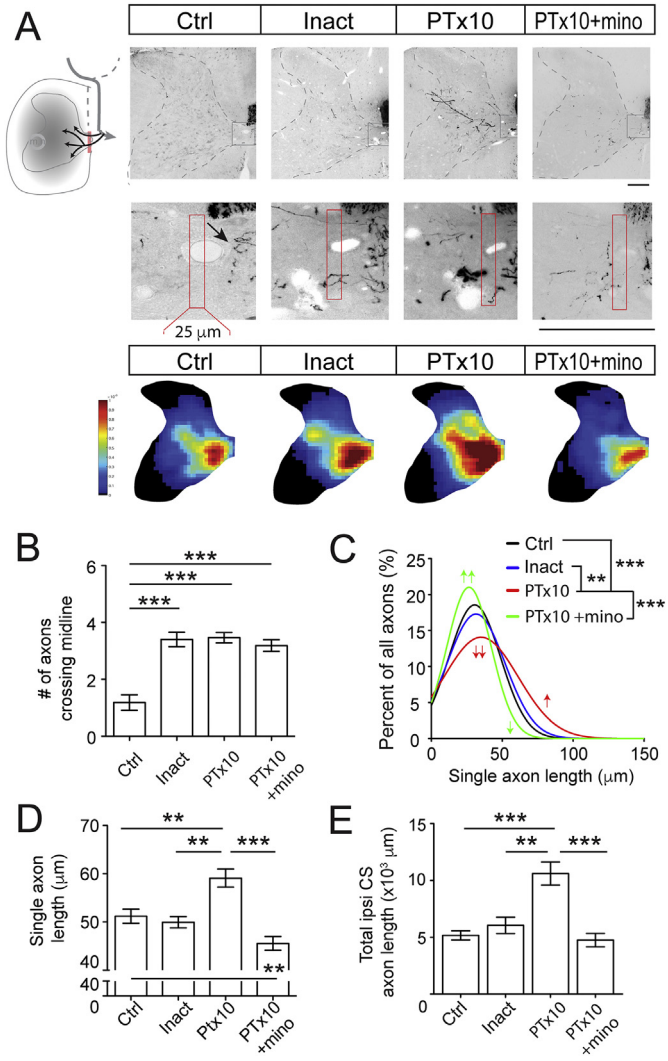

Fig. 3. The midline-crossing capability, but not elongation, of ipsilateral CST axons is equally potentiated after MCX inactivation, PTx- and combined minocycline-and PTx. A. Representative images and heatmaps of BDA-labeled ipsilateral CST axons. The schematic on the left shows axons re-crossing the midline to enter the affected (denervated/inactivated; gray) spinal cord gray matter, where the axons could branch and elongate to project to different areas. The red rectangle marks the area for counting of midline-crossing axons. Upper panel: lower magnification images show greater ipsilateral CST axons in the gray matter of the PTx group compared to all other groups. Middle panel: high magnification of ipsilateral lamina X region, indicated in upper images, showing midline crossing axons. The rectangular area was used for axon counting. Arrow indicates that contralateral CS axons make hairpin-like turns at the midline in the control. Scale: 0.2 mm. Lower panel: heatmaps of ipsilateral CST axons showing the marked increase in density of ipsilateral CST axons after PTx, but not after MCX inactivation. Minocycline treatment blocked the increase after PTx. Colour scale represents normalized pixel densities. The scale is the same for all heat maps (1×10^{-3}). B. Quantification of the number of axons crossing the lamina 10 boundary in a 40 μm thick section shows similar changes among all groups. All treatments equally and significantly elevated midline axon crossing (Kruskal-Wallis test, $P < .0001$; Dunn's multiple comparison test: ***P < .0001). C. Frequency distribution curves for single axon length analysis (K–S test, ***P < .0001, **P < .01). D. Group comparisons for averaged single axon gray matter length analysis. PTx, but not MCX inactivation, induced significant axonal elongation, which is blocked by minocycline (Kruskal-Wallis test, P < .0001; Dunn's multiple comparison test: ***P < .0001, **P < .01). E. Total length of ipsilateral CST axons in the gray matter. PTx, but not MCX inactivation, induced significant axonal elongation, which is blocked by minocycline (Kruskal-Wallis test, P < .0001; Dunn's multiple comparison test: ***P = .0001, **P < .01). (For interpretation of the references to colour in this figure legend, the reader is referred to the web version of this article.)

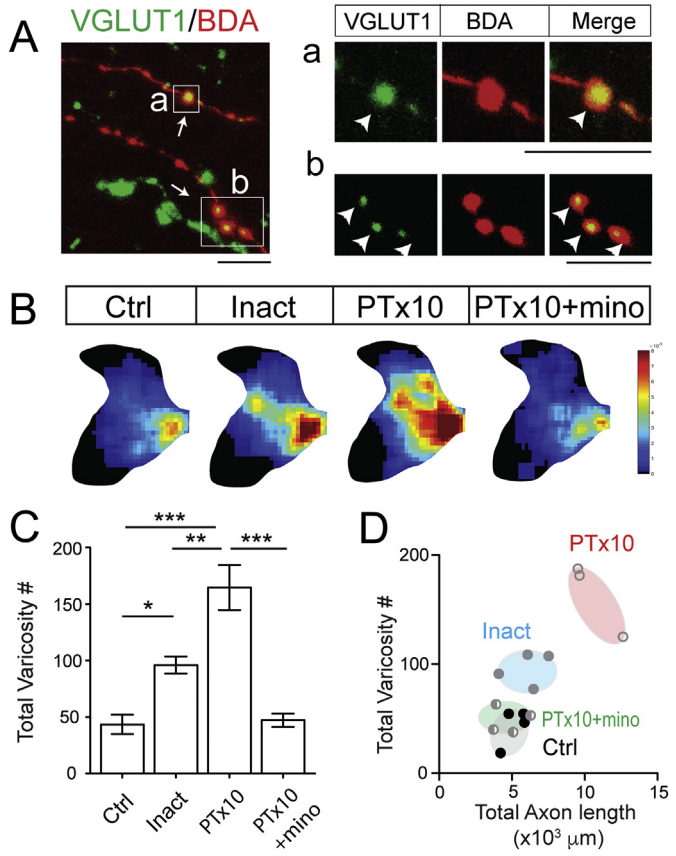

Fig. 4. MCX inactivation potentiates the formation of new presynaptic sites on ipsilateral CST axons, which is more prominent after PTx and is blocked by minocycline. A. Representative images showing co-labeling of BDA positive ipsilateral CST axon varicosities (red, arrows) with excitatory presynaptic terminal marker for CST axons, VGLUT1 (green, arrow heads). Projection of z stack confocal images (left) and enlarged single optical plane images of square areas (a and b) are shown. Scale: 10 μm. B. Heatmaps of ipsilateral CST axon varicosities showing the change in density and distribution pattern. Both MCX inactivation and PTx increased the varicosity density and territories. Minocycline treatment blocked the increase after PTx. The scale is the same for all heat maps (8×10^{-5}). C. Quantification of the varicosity densities of ipsilateral CST axons show a significant increase after both MCX inactivation and PTx. The response after PTx is completely abolished with minocycline treatment (One-way ANOVA analysis, $p < .0001$; Tukey's multiple comparison test, *p < .05, **p < .01, ***p < .001). D. The association between total axon length and varicosity numbers for ipsilateral CST axons in individual animals from the different groups (PTx10, open circles; Inactivation; filled gray circles; PTx10 + minocycline, half open and gray; Control, filled black circles). MCX inactivation primarily promotes formation of new presynaptic sites from the unaffected CST, whereas PTx additionally drives axonal elongation. Minocycline treatment blocks both processes after PTx. (For interpretation of the references to colour in this figure legend, the reader is referred to the web version of this article.)

crossing, but was necessary for individual gray matter axon elongation.

3.4. Gray matter CST terminations are differentially potentiated in response to inactivation and PTx and blocked by minocycline after PTx

After PTx, the activity-dependent increase in crossing axons and the elongation of axons—which depends on injury-associated inflammation, including microglial activation—could contribute to reconstruction of the connections of spared CST axons within the denervated spinal cord gray matter. We next determined if CST denervation produced changes in the topography and regional density of presynaptic sites. CST presynaptic terminals are morphologically characterized as

axonal varicosities, defined as a tracer-filled 3-fold (or greater) widening of the axon (Fig. 4A, left; arrows in the z-stack of optical images). As we have previously shown, CST axon varicosities co-label with VGLUT1 (Fig. 4A, a and b; arrow heads in single plane images), which mark their excitatory presynaptic boutons. Taking advantage of their morphological characteristic, we marked CST axon varicosities along traced axons, and constructed regional density heatmaps to show changes in the topographic distribution of putative presynaptic sites across animal groups (Fig. 4B). In control animals, ipsilateral CST axon terminals are normally sparse and largely restricted to the medial intermediate zone and medial ventral horn. Immediately after 10 days of MCX inactivation, despite the lack of significant CST axonal elongation (Fig. 3C and E), there is a larger increase in axon varicosities in the ventromedial area, a small diffuse increase laterally in the intermediate zone and dorsal horn, and a new strong focus in the lateral dorsal horn. Ten days after PTx, there is a further increase in ventromedial, dorsolateral, and dorsomedial varicosity labeling. The quantification of total number of varicosities showed a 121% increase after 10 days of MCX inactivation and a 279% increase after PTx compared with the control group (Fig. 4C. ctrl: 43.4 ± 8.5, inact: 96.1 ± 7.5, PTx10: 164.6 ± 19.9; One Way ANOVA analysis, $p < .0001$; Tukey's multiple comparison test, $^{*}p < .05$, $^{**}p < .01$, ***p < .001). In addition, minocycline treatment completely abolished the varicosity increase after PTx (47.2 ± 6.0, ***p < .001). These findings suggest that selective cortical inactivation is sufficient to drive spared CST axons to form new putative synaptic connections, largely along their original axons. The further varicosity increase after PTx may reflect the concurrent axon elongation. The findings further indicate that in addition to activity loss robust injury-induced inflammation, including microglial activation, is also required for the formation of a greater number of new varicosities after injury.

To summarize the changes in total CST axon length and varicosity numbers after different CST manipulation, we plotted the two values from individual animals (Fig. 4D). The data points of PTx10 animals occupy the top right compartment of the figure due to greater axon length and higher varicosity numbers. The values of MCX inactivation animals are much higher in varicosity density than controls but less so for axon length than after PTx10, and thus locate in the middle left portion of the plot. Minocycline treatment shifted the values of PTx10 animals to the lower left corner, similar to control values, due to both shorter axon lengths and lower varicosity numbers. This representation of the data shows that activity loss in the target side of the spinal cord is critically involved in the formation of putative synapses on spared CST axons, but not for axonal elongation. This, in turn, seems to constrain the increase in total number of putative presynaptic sites compared to PTx. Moreover, our findings show that injury-induced inflammation supports the formation of new connections after PTx by enabling greater axonal elongation.

3.5. Reactive sprouting of proprioceptive afferents in response to CST denervation and minocycline treatment

In addition to the sprouting of CST axons produced by inactivation or PTx, proprioceptive afferents (PA) also show increased gray matter innervation after PTx, as shown in our earlier study (Tan et al., 2012). Here, we investigated the activity- and microglial-dependence of this response. We studied proprioceptive afferents from the extensor carpi radialis muscle (ECR) as the target muscle due to its large MCX representation (Brus-Ramer et al., 2009). We traced ECR proprioceptive afferents using transganglionic transport of CTB. In a subset of animals, we co-labeled CTB with VGLUT1, the glutamate transporter for large-diameter afferents (Alvarez et al., 2004), and found that CTB+ clusters stain with VGLUT1 (Fig. 5A). This indicates that marking of CTB positive puncta well-represents the presynaptic terminals of ECR proprioceptive afferents. In turn, we reason that a change in the density of CTB+ clusters indicates a change in PA presynaptic terminals.

We captured changes in CTB cluster density both as heatmaps (Fig. 5B-E) and as mediolateral CTB density distributions (Fig. 5F, G). We compared the distribution of proprioceptive terminals after MCX inactivation, PTx10, and after PTx10 + minocycline. We verified that CTB labeling across groups was not different by comparing the numbers of retrogradely-labeled ECR motoneurons in the ventrolateral motor neuron pool on both sides of the spinal cord within animals, and across all groups (Fig. 5B to E). Proprioceptive ECR afferents showed a dense band across laminae III to IV, which did not seem to differ across groups. In contrast, labeling in laminae V to VII increased after cortical inactivation (Fig. 5C) and more so after PTx10 (Fig. 5D). Interestingly, the increases were topographically distinct, with inactivation elevating PA terminations laterally (Fig. 5Cii) and PTX, medially (Fig. 5Dii). Minocycline treatment completely abolished the medial CTB increase in PTx animals (Fig. 5E). These topographic distribution patterns and changes are well-demonstrated by the mediolateral distribution curves, which were also fitted to Gaussian distributions (Fig. 5F). Compared with the relatively even mediolateral distribution pattern in control animals (black curve), MCX inactivation resulted in a laterally-centered elevated peak in CTB labeling (blue curve, K−S test, $p < .0001$). In contrast, PTx produced a medial-centered peak (red curve, K−S test to control: p < .0001). Minocycline treatment after PTX prevented the robust sprouting response after PTX (green curve, K−S test, p < .0001). The area under the lateral and medial parts of the curves (AUC; dotted line, Fig. 5F) was measured, respectively, and summarized (Fig. 5G). CTB staining in the inactivation group (lateral) nearly doubled compared with lateral labeling in controls, and the PTx10 medial CTB signal showed nearly a 6-times increase compared with medial labeling in controls. Total CTB label in the inactivation animals (lateral) was not different from the total PTx labeling (medial). Minocycline treatment largely eliminated the increase in CTB signal in the medial intermediate zone in PTx10 animals (AUC, Kruskal-Wallis test, $P < .0001$; Dunn's multiple comparison test: $^{**}P < .01$, $^{***}P < .001$). These findings show that changes in ECR proprioceptive terminals are similar to those of spared CST axons. They together suggest that cortical inactivation can trigger formation of new PA fiber connections nearly as efficiently as PTx at remote locations, and this requires support of injury-induced inflammation, especially activated microglia cells.

3.6. Overlap of the areas of ipsilateral corticospinal and proprioceptive terminals in spinal cord

Proprioceptive afferents and descending motor pathways, including the CST, are the two major classes of extrinsic inputs to spinal segmental motor circuits; they closely interact with each other during postural control, locomotion, and voluntary movements (Dietz, 2002). The parallel sprouting of proprioceptive afferents and CST axons in response to CS system manipulation, either by MCX inactivation or PTx, is different from competition between bilateral CST pathways during development (Martin and Lee, 1999), or between contralateral CST axons and PAs that we observed previously (Jiang et al., 2016). This prompted us to examine whether there is any topographic association between the location of the spared CST and PA labeling in spinal gray matter with a focus in lamina VI to VII, where there are projections from both inputs. We first co-labled CST and PA axons in the denervated spinal cord (Fig. 6A-C). Similar to what we described previously, both ipsilateral CST and PA axons are very sparse in lamina V to VII of control spinal cord (Fig. 6Ai and ii) and there is minimal overlap between them, as shown on a representative single section (Fig. 6Aiii). After MCX inactivation, there is a small increase in active CS axons and PA terminals in same area of lateral deep dorsal horn (arrow head in fig. 6Biii). PTx drives a larger projection from PA and spared CST axons to both medial and lateral deep dorsal horn (arrows in fig. 6Ciii). We then warped the varicosity heatmaps of the spared CST and PA terminations that we presented earlier to enable direct topographic comparison

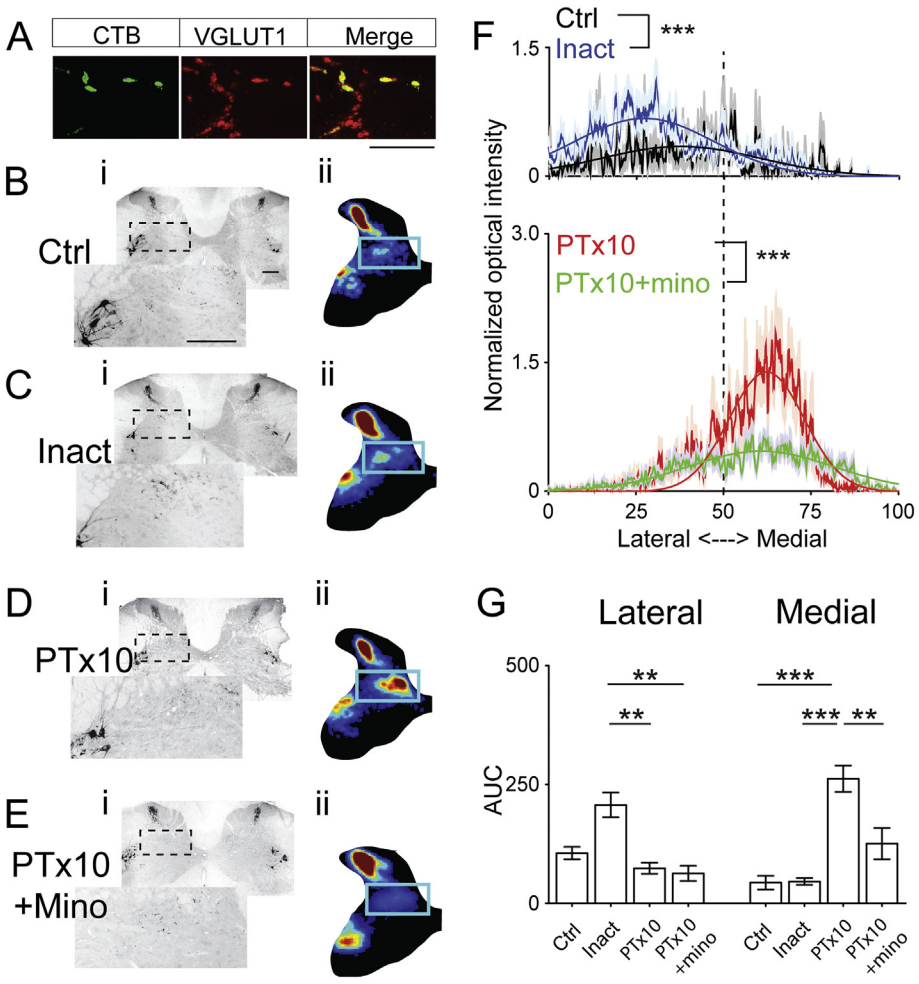

Fig. 5. Muscle proprioceptive afferents sprout in response to M1 inactivation and PTx. A. Colocalization of CTB+ ECR proprioceptive afferent terminals (green) with the excitatory presynaptic terminal marker, VGLUT1+ (red). Scale: 10 μm. B to E. Representative images (i) and density heatmaps (ii) of CTB traced ECR proprioceptive afferent terminals in the spinal cord. Note that there are more CTB positive terminals in the lateral deep dorsal horn in the MCX inactivation animals (Ci and ii), which expanded to the medial deep dorsal horn after PTx (Di and ii). CTB signal is much lower in the deep dorsal horn in the PTx + minocycline treated group (Ei and ii). Scale: 0.2 mm. F. Mediolateral distributions of CTB signal in the deep dorsal horn showed significantly increased signal laterally after inactivation, and medially after PTx; minocycline abolished the increase after PTx (K–S test, $p < .0001$). G. Quantification of area under the medial or lateral half of the mediolateral distribution curves, respectively. The integrated CTB signal significantly increased laterally after MCX inactivation, and medially after PTx, minocycline significantly suppressed the increase after PTx (Kruskal-Wallis test, $p < .0001$, Dunn's multiple comparison, *** $p < .001$, ** $p < .01$, * $p < .05$). (For interpretation of the references to colour in this figure legend, the reader is referred to the web version of this article.)

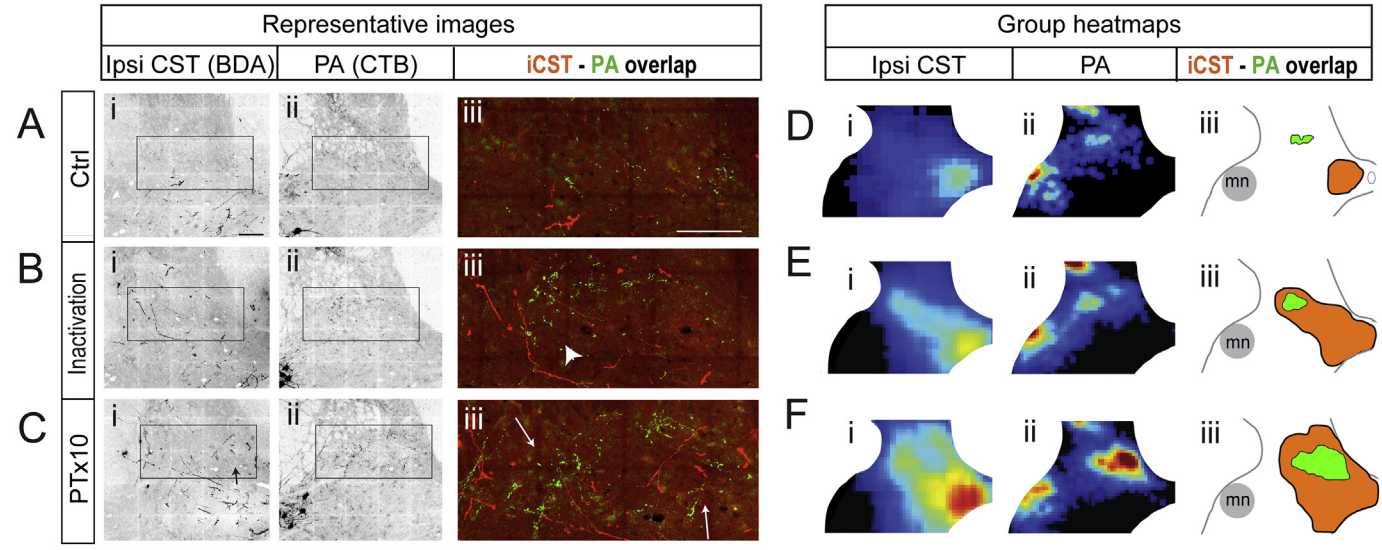

Fig. 6. The territories of newly formed ipsilateral CST axon varicosities and proprioceptive afferent terminals overlap within the spinal cord after MCX inactivation and PTx. A-C. Co-labeling of ipsilateral CST (BDA, i) and PA (CTB, ii) in control (A), inactivation (B) and PTx10 (C) spinal cords. The merged images (iii, red for CST, green for PA.) show topographic overlap between the two pathways (arrow head in 6Biii, arrows in 6Ciii). Scale: 0.2 mm. D-F. The ipsilateral CST varicosities (i) and CTB labeled ECR-PA terminal (ii) density heatmaps were warped into the same gray matter size/shape and compared within controls (D), MCX inactivation (E) and PTx groups (F) individually. The termination territory of each pathway is summarized in iii (green, ECR-PA terminals; orange, for ipsi-CST varicosities). The boundaries correspond to the bright blue area. The ECR motor pool is shown in gray. (For interpretation of the references to colour in this figure legend, the reader is referred to the web version of this article.)

(Fig. 6D-F, i and ii). We compared the high-density areas of the terminations from each pathway (corresponding to bright blue colour, Fig. 6D-F, iii). Consistent with the double-labeled images, there is no overlap between spared CST and PA termination in control animals (Fig. 6Diii). MCX inactivation drove nearly complete topographic overlap in the lateral deep dorsal horn (Fig. 6Eiii). This overlap expanded into the medial dorsal horn in PTx animals (Fig. 6Fiii). The segregation of overlap zones in medial and lateral deep dorsal is likely related to the targets of CS manipulations. Cortical inactivation disrupted CST axons from MCX only, which primarily terminate in the lateral intermediate zone of spinal cord, while PTx disrupted CST axons from both MCX and the somatic sensory cortex; the sensory projection is predominantly to the more medial intermediate zone (Ueno et al., 2018; Kameda et al., 2019). The overlap of spared CST and PA terminals, although somewhat different in individual groups, suggests that they may be affected similarly when encountering activity manipulation of spinal motor circuits; mildly by MCX inactivation and strongly by PTx. The emergent anatomical overlap may enable interactions between the two new pathways in the spinal sensorimotor circuit.

4. Discussion

Spared axonal sprouting in the spinal cord mechanistically may underlie motor recovery after injury, which is a gain of function, as well as hyperreflexia, a gain of dysfunction. Since most spinal cord injuries are incomplete, promoting adaptive sprouting of spared descending axons after injury is a potential target for motor repair to foster voluntary control. In this study, using MCX inactivation to silence the forelimb area, which gives rise to a portion of the cervical CST projection, we show a significant and substantial contribution of activity loss to the triggering of CST sprouting into the affected side of spinal cord and subsequent formation of putative synapses. PA sprouting also was augmented with activity loss. Axon elongation and synapse formation, from the CST and PAs alike, was further dependent on injury-induced inflammation, including microglial phagocytosis of myelin debris in spinal cord, which is far from the primary injury site. Our findings suggest that an important component of CST and PA sprouting on the denervated side of the spinal cord is due to the loss of activity that occurs as a consequence of the injury. And our data further suggest possible distinctive roles for neural activity and inflammatory responses, in mature axonal outgrowth, including guidance, elongation, and synaptogenesis. Combining an activity-promoting manipulation and inflammation control may help achieve better functional restoration after injury than either alone.

4.1. Changes in neuronal activity trigger spinal circuit rewiring

Neuronal activity is known to be pivotal for axonal plasticity and circuit reorganization during development and in maturity (Katz and Shatz, 1996; Martin and Lee, 1999). In our study, for the first time, we suggest three component steps towards CST axonal growth to its terminal field in the spinal gray matter, based on comparison of the characteristics of these steps produced by forelimb MCX inactivation and PTx. We show that the loss of activity is capable of triggering CST axon outgrowth across the midline towards the side with reduced activity. Presumably, this is related to controlling the guidance of the sprouting axon, including the initial direction (i.e., increased crossing axon numbers), the eventual termination within a particular territory in the intermediate zone and dorsal horn, as well as the density of the terminals. The capacity for spared axonal outgrowth and guidance to the affected side are equally strengthened following forelimb MCX inactivation and PTx, which would produce an immediate loss of post-synaptic target circuit activity. These findings strongly support our hypothesis that the loss of activity, while likely not the only factor, is an essential trigger for axonal sprouting after injury. The activity change not only determines the capacity for sprouting, but may also bias that growth towards the inactive/denervated side.

It is important to recognize that inactivation did not produce a lesion. Whereas the injection cannula would displace and possibly damage MCX cells at the implantation site, we previously found that labeled CST neurons are present close to the cannula tract (Martin et al., 1999). And in our present study, there was no microglial activation and no loss of PKCγ-labeled inactivated CST axons in the dorsal column, as after PTx. These observations point to a lack of direct injury to CST axons, and thus activity suppression is the major driven for circuit reorganization. More interesting, we observed significantly increased microglial phagocytosis of myelin (MBP), but not inactivated CST axonal debris (BDA), in the contralateral spinal cord after MCX inactivation. This strongly suggests that an activity dependent demyelination, but not axon loss, was primarily induced by activity suppression. This not only might open up space for the formation of new connections by axonal demyelination, but the preservation of inactivated axons also enables more dynamic modulation of manipulated axons as we found previously; where the return of activity quickly brings back normal functional connections (Jiang et al., 2016).

Our finding that activity loss mimics connection loss after injury helps to explain transcallosal sprouting after unilateral stroke (Carmichael and Chesselet, 2002). In a rat model with a unilateral thremocoagulation lesion in sensorimotor cortex, increased low frequency synchronized neuronal activity was present in the peri-lesion cortex early after injury, and then in the contralesional cortex, where axonal sprouting occurs. The synchronized neuronal activity in peri-lesion cortex is similar to the patterned activity in the developing retina, hippocampus, and cortex, which is known to be pivotal for circuit formation (Katz and Shatz, 1996; Stellwagen and Shatz, 2002; Egorov and Draguhn, 2013). Indeed, activity blockade in the peri-lesion cortex abrogates the contralesional sprouting (Carmichael and Chesselet, 2002), implying a direct association between increased activity with axonal sprouting and circuit rewiring in the spared ipsilateral cortex. It is plausible that unilateral PTx or MCX inactivation also leads to increased activity in the intact MCX, which gives the spared forelimb CST axons a competitive advantage in gaining synaptic target space in the spinal cord (Jiang et al., 2016). A similar mechanism may also apply to the sprouting of spared PA pathways, due to its close interaction with the CST (Chakrabarty and Martin, 2011). It will be interesting to look directly at the neuronal activity of spared CST pathway and PAs in our cortical inactivation and PTx models. This idea is consistent with our MCX stimulation-based intervention to promote sprouting of spared CST axons and function after injury (Brus-Ramer et al., 2007; Carmel et al., 2014).

4.2. Targeting injury-induced inflammation and microglial activation by minocycline abrogates establishment of expanded PA and spared ipsilateral CST terminations after PTx

Neuroinflammation typically develops following spinal cord and brain injury, which is induced by Wallerian degeneration of damaged axons (George and Griffin, 1994; Chen and Shine, 2013). Despite the traditional known destructive effects of neuroinflammation (Fitch and Silver, 2008; Jiang et al., 2018), an increasing number of studies have revealed constructive effects of neuroinflammation in post-injury repair. For example, eliciting additional inflammatory responses in injured animals by systemic injection of LPS was found to decrease the size of lesion cavities (Guth et al., 1994; Popovich et al., 2012), and increase spared axonal sprouting near the injury sites (Popovich et al., 2012; Torres-Espin et al., 2018). Since these studies mostly focus on the injury sites or nearby tissue, peripheral macrophages and circulating immune cells are considered to be the major functional cell types contributing to these effects (Schnell et al., 1999; Babcock et al., 2003). Our study differs from the others in three ways. First, we studied the cervical spinal cord, which is far from the medullary lesion. Because this is not the lesion site, microglia cells are likely the major player here

(Popovich et al., 1997). Second, we used chronic application of minocycline, a widely used anti-inflammation drug (Garrido-Mesa et al., 2013) targeting endogenously activated inflammatory responses. Third, with step-by-step comparisons, we found that minocycline treatment blocked the formation of axon elongation in the gray matter after injury, and associated presynaptic site formation, without much of an effect on the enhanced midline axon re-crossing. These findings strongly suggest the presence of a sufficiently robust post-injury inflammatory response, most likely produced by microglia at remote spinal locations. In turn, this inflammatory response supports axon sprouting triggered by activity, enabling expansion of gray matter axonal projections and establishment of more synaptic connections.

Several mechanisms are considered to be involved in the supportive function of neuroinflammation on axon sprouting. One is increased phagocytosis performed by activated microglial cells (Czeh et al., 2011), as we showed in this study. This process not only vacates spaces for axon growth, but more important, it eliminates the growth-inhibiting molecules produced by degenerated myelin tissue, such as Nogo (Chen et al., 2000; Neumann et al., 2009). Insufficient phagocytosis of degenerated tissue has been shown to interfere with axonal outgrowth and functional recovery (Neumann et al., 2009; Lampron et al., 2015). We found parallel changes in microglial phagocytosis of myelin debris and axonal sprouting after PTx, with or without minocycline treatment, which strongly implies the positive association of microglial phagocytosis with axonal sprouting. In animals with cortical inactivation, although we did not observe injury-induced microglial proliferation in the dorsal column, the phagocytosis of MBP by microglial cells increased in the gray matter where inactivated CST axons project, which suggests that inactivation is able to drive mild activity-dependent demyelination and subsequent neuroinflammation. And this may partially contribute to the formation of new presynaptic sites on spared CS and PA axons.

With that being said, we do not exclude the contribution of other supportive functions of microglial cells—as well as circulating immune cells, which also can be targeted by systemic minocycline. Both microglia and T lymphocytes are able to produce neurotrophins, and anti-inflammatory cytokines that stimulate axon sprouting (Batchelor et al., 2002; Chen and Shine, 2013). Activated microglia may also indirectly increase neuronal activity, by stimulating astrocytes to release the excitatory neurotransmitter glutamate (Pascual et al., 2012), or ensheathing neurons to displace inhibitory synapses (Chen et al., 2014). All of the above mechanisms would be expected to promote spared axonal sprouting after injury (Kumar and Loane, 2012) and would be blocked by minocycline treatment.

4.3. Functional significance of activity and neuroinflammation-dependent axonal sprouting

Axon sprouting after injury is typically associated with function change. Spontaneous sprouting of spared CST (Weidner et al., 2001) and descending brain stem pathways (Bachmann et al., 2014) are associated with motor behavioral improvement after injury. On the other hand, PA sprouting is associated more with the development of dysfunction because it contributes to the hyperreflexia after PTx (Tan et al., 2012) and muscle spasms after SCI (Dietz, 2002). In our study, sprouting of spared CST and PA axons—which contribute to gain of adaptive and maladaptive functions, respectively—are similarly modulated by neuronal activity and neuroinflammation, and seemingly interrelated. These adaptive and maladaptive gains in functions are achieved by overlapped sprouting of the two pathways, which underlie the complexity of post-injury physiological changes and the determinants of functional recovery.

That different spinal inputs respond similarly to activity and inflammation is also a challenge for rehabilitation. When we try to promote CST axons to sprout to compensate for lost descending motor inputs, we need to avoid development of hyperreflexia that is associated with PA sprouting (Tan et al., 2012). Systemic minocycline, for instance, showed inconsistent rehabilitation effects in spinal cord injury patients in clinical trials (Casha et al., 2012). This may be due to simultaneously preventing the benefits of spared CST sprouting and the disadvantages of PA sprouting. This urges us to explore pathway-specific interventions in functional rehabilitation.

Acknowledgments

We thank Xiuli Wu for histology. This work was supported by the NIH (JHM: 2R01NS064004), the Craig H. Neilsen Foundation (JHM: 261214), and the New York State Department of Health Spinal Cord Injury Research Board (JHM: C030606GG).

References

Alvarez, F.J., Villalba, R.M., Zerda, R., Schneider, S.P., 2004. Vesicular glutamate transporters in the spinal cord, with special reference to sensory primary afferent synapses. J. Comp. Neurol. 472, 257–280.
Ando, S., Tanaka, Y., Toyoda, Y., Kon, K., 2003. Turnover of myelin lipids in aging brain. Neurochem. Res. 28, 5–13.
Babcock, A.A., Kuziel, W.A., Rivest, S., Owens, T., 2003. Chemokine expression by glial cells directs leukocytes to sites of axonal injury in the CNS. J. Neurosci. 23, 7922–7930.
Bachmann, L.C., Lindau, N.T., Felder, P., Schwab, M.E., 2014. Sprouting of brainstem-spinal tracts in response to unilateral motor cortex stroke in mice. J. Neurosci. 34, 3378–3389.
Bareyre, F.M., Kerschensteiner, M., Raineteau, O., Mettenleiter, T.C., Weinmann, O., Schwab, M.E., 2004. The injured spinal cord spontaneously forms a new intraspinal circuit in adult rats. Nat. Neurosci. 7, 269–277.
Batchelor, P.E., Porritt, M.J., Martinello, P., Parish, C.L., Liberatore, G.T., Donnan, G.A., Howells, D.W., 2002. Macrophages and microglia produce local trophic gradients that stimulate axonal sprouting toward but not beyond the wound edge. Mol. Cell. Neurosci. 21, 436–453.
Brooks, V.B., Stoney Jr., S.D., 1971. Motor mechanisms: the role of the pyramidal system in motor control. Annu. Rev. Physiol. 33, 337–392.
Brus-Ramer, M., Carmel, J.B., Chakrabarty, S., Martin, J.H., 2007. Electrical stimulation of spared corticospinal axons augments connections with ipsilateral spinal motor circuits after injury. J. Neurosci. 27, 13793–13801.
Brus-Ramer, M., Carmel, J.B., Martin, J.H., 2009. Motor cortex bilateral motor representation depends on subcortical and interhemispheric interactions. J. Neurosci. 29, 6196–6206.
Carmel, J.B., Kimura, H., Martin, J.H., 2014. Electrical stimulation of motor cortex in the uninjured hemisphere after chronic unilateral injury promotes recovery of skilled locomotion through ipsilateral control. J. Neurosci. 34, 462–466.
Carmichael, S.T., Chesselet, M.F., 2002. Synchronous neuronal activity is a signal for axonal sprouting after cortical lesions in the adult. J. Neurosci. 22, 6062–6070.
Casha, S., Zygun, D., McGowan, M.D., Bains, I., Yong, V.W., Hurlbert, R.J., 2012. Results of a phase II placebo-controlled randomized trial of minocycline in acute spinal cord injury. Brain 135, 1224–1236.
Chakrabarty, S., Martin, J.H., 2011. Co-development of proprioceptive afferents and the corticospinal tract within the cervical spinal cord. Eur. J. Neurosci. 34, 682–694.
Chen, Q., Shine, H.D., 2013. Neuroimmune processes associated with Wallerian degeneration support neurotrophin-3-induced axonal sprouting in the injured spinal cord. J. Neurosci. Res. 91, 1280–1291.
Chen, M.S., Huber, A.B., van der Haar, M.E., Frank, M., Schnell, L., Spillmann, A.A., Christ, F., Schwab, M.E., 2000. Nogo-a is a myelin-associated neurite outgrowth inhibitor and an antigen for monoclonal antibody IN-1. Nature 403, 434–439.
Chen, Q., Smith, G.M., Shine, H.D., 2008. Immune activation is required for NT-3-induced axonal plasticity in chronic spinal cord injury. Exp. Neurol. 209, 497–509.
Chen, Z., Jalabi, W., Hu, W., Park, H.J., Gale, J.T., Kidd, G.J., Bernatowicz, R., Gossman, Z.C., Chen, J.T., Dutta, R., Trapp, B.D., 2014. Microglial displacement of inhibitory synapses provides neuroprotection in the adult brain. Nat. Commun. 5, 4486.
Czeh, M., Gressens, P., Kaindl, A.M., 2011. The yin and yang of microglia. Dev. Neurosci. 33, 199–209.
Dietz, V., 2002. Proprioception and locomotor disorders. Nat. Rev. Neurosci. 3, 781–790.
Egorov, A.V., Draguhn, A., 2013. Development of coherent neuronal activity patterns in mammalian cortical networks: common principles and local hetereogeneity. Mech. Dev. 130, 412–423.
Filipp, M.E., Travis, B.J., Henry, S.S., Idzikowski, E.C., Magnuson, S.A., Loh, M.Y., Hellenbrand, D.J., Hanna, A.S., 2019. Differences in neuroplasticity after spinal cord injury in varying animal models and humans. Neural Regen. Res. 14, 7–19.
Fitch, M.T., Silver, J., 2008. CNS injury, glial scars, and inflammation: inhibitory extracellular matrices and regeneration failure. Exp. Neurol. 209, 294–301.
Garrido-Mesa, N., Zarzuelo, A., Galvez, J., 2013. Minocycline: far beyond an antibiotic. Br. J. Pharmacol. 169, 337–352.
George, R., Griffin, J.W., 1994. Delayed macrophage responses and myelin clearance during Wallerian degeneration in the central nervous system: the dorsal radiculotomy model. Exp. Neurol. 129, 225–236.
Greenhalgh, A.D., David, S., 2014. Differences in the phagocytic response of microglia and peripheral macrophages after spinal cord injury and its effects on cell death. J.

Neurosci. 34, 6316–6322.
Guth, L., Zhang, Z., DiProspero, N.A., Joubin, K., Fitch, M.T., 1994. Spinal cord injury in the rat: treatment with bacterial lipopolysaccharide and indomethacin enhances cellular repair and locomotor function. Exp. Neurol. 126, 76–87.
Jiang, Y.Q., Williams, P.T., Martin, J.H., 2013. Rapid and persistent impairments of the forelimb motor representations following cervical deafferentation in rats. Eur. J. Neurosci. 38, 3702–3711.
Jiang, Y.Q., Zaaimi, B., Martin, J.H., 2016. Competition with primary sensory afferents drives Remodeling of Corticospinal axons in mature spinal motor circuits. J. Neurosci. 36, 193–203.
Jiang, Y.Q., Sarkar, A., Amer, A., Martin, J.H., 2018. Transneuronal down-regulation of the premotor cholinergic system after corticospinal tract loss. J. Neurosci. 38, 8329–8344.
Kameda, H., Murabe, N., Odagaki, K., Mizukami, H., Ozawa, K., Sakurai, M., 2019. Differential innervation within a transverse plane of spinal gray matter by sensorimotor cortices, with special reference to the somatosensory cortices. J. Comp. Neurol. 527, 1401–1415.
Katz, L.C., Shatz, C.J., 1996. Synaptic activity and the construction of cortical circuits. Science 274, 1133–1138.
Kumar, A., Loane, D.J., 2012. Neuroinflammation after traumatic brain injury: opportunities for therapeutic intervention. Brain Behav. Immun. 26, 1191–1201.
Lampron, A., Larochelle, A., Laflamme, N., Prefontaine, P., Plante, M.M., Sanchez, M.G., Yong, V.W., Stys, P.K., Tremblay, M.E., Rivest, S., 2015. Inefficient clearance of myelin debris by microglia impairs remyelinating processes. J. Exp. Med. 212, 481–495.
Lang, C., Bradley, P.M., Jacobi, A., Kerschensteiner, M., Bareyre, F.M., 2013. STAT3 promotes corticospinal remodelling and functional recovery after spinal cord injury. EMBO Rep. 14, 931–937.
Lazarov-Spiegler, O., Solomon, A.S., Zeev-Brann, A.B., Hirschberg, D.L., Lavie, V., Schwartz, M., 1996. Transplantation of activated macrophages overcomes central nervous system regrowth failure. FASEB J. 10, 1296–1302.
Lee, D.H., Luo, X., Yungher, B.J., Bray, E., Lee, J.K., Park, K.K., 2014. Mammalian target of rapamycin's distinct roles and effectiveness in promoting compensatory axonal sprouting in the injured CNS. J. Neurosci. 34, 15347–15355.
Lemon, R.N., 2008. Descending pathways in motor control. Annu. Rev. Neurosci. 31, 195–218.
Lindau, N.T., Banninger, B.J., Gullo, M., Good, N.A., Bachmann, L.C., Starkey, M.L., Schwab, M.E., 2014. Rewiring of the corticospinal tract in the adult rat after unilateral stroke and anti-Nogo-a therapy. Brain J. Neurol. 137, 739–756.
Martin, J.H., 2005. The corticospinal system: from development to motor control. Neuroscientist 11, 161–173.
Martin, J.H., Ghez, C., 1999. Pharmacological inactivation in the analysis of the central control of movement. J. Neurosci. Methods 86, 145–159.
Martin, J.H., Lee, S.J., 1999. Activity-dependent competition between developing corticospinal terminations. Neuroreport 10, 2277–2282.
Martin, J.H., Kably, B., Hacking, A., 1999. Activity-dependent development of cortical axon terminations in the spinal cord and brain stem. Exp. Brain Res. 125, 184–199.
Neumann, H., Kotter, M.R., Franklin, R.J., 2009. Debris clearance by microglia: an essential link between degeneration and regeneration. Brain J. Neurol. 132, 288–295.
Nimmerjahn, A., Kirchhoff, F., Helmchen, F., 2005. Resting microglial cells are highly dynamic surveillants of brain parenchyma in vivo. Science 308, 1314–1318.
Parkhurst, C.N., Yang, G., Ninan, I., Savas, J.N., Yates 3rd, J.R., Lafaille, J.J., Hempstead, B.L., Littman, D.R., Gan, W.B., 2013. Microglia promote learning-dependent synapse formation through brain-derived neurotrophic factor. Cell 155, 1596–1609.
Pascual, O., Ben Achour, S., Rostaing, P., Triller, A., Bessis, A., 2012. Microglia activation triggers astrocyte-mediated modulation of excitatory neurotransmission. Proc. Natl. Acad. Sci. U. S. A. 109, E197–E205.
Popovich, P.G., Longbrake, E.E., 2008. Can the immune system be harnessed to repair the CNS? Nature reviews. Neuroscience 9, 481–493.
Popovich, P.G., Wei, P., Stokes, B.T., 1997. Cellular inflammatory response after spinal cord injury in Sprague-Dawley and Lewis rats. J. Comp. Neurol. 377, 443–464.
Popovich, P.G., Tovar, C.A., Wei, P., Fisher, L., Jakeman, L.B., Basso, D.M., 2012. A reassessment of a classic neuroprotective combination therapy for spinal cord injured rats: LPS/pregnenolone/indomethacin. Exp. Neurol. 233, 677–685.
Riva-Depaty, I., Fardeau, C., Mariani, J., Bouchaud, C., Delhaye-Bouchaud, N., 1994. Contribution of peripheral macrophages and microglia to the cellular reaction after mechanical or neurotoxin-induced lesions of the rat brain. Exp. Neurol. 128, 77–87.
Safaiyan, S., Kannaiyan, N., Snaidero, N., Brioschi, S., Biber, K., Yona, S., Edinger, A.L., Jung, S., Rossner, M.J., Simons, M., 2016. Age-related myelin degradation burdens the clearance function of microglia during aging. Nat. Neurosci. 19, 995–998.
Schnell, L., Fearn, S., Klassen, H., Schwab, M.E., Perry, V.H., 1999. Acute inflammatory responses to mechanical lesions in the CNS: differences between brain and spinal cord. Eur. J. Neurosci. 11, 3648–3658.
Schwab, M.E., 2002. Increasing plasticity and functional recovery of the lesioned spinal cord. Prog. Brain Res. 137, 351–359.
Shultz, R.B., Zhong, Y., 2017. Minocycline targets multiple secondary injury mechanisms in traumatic spinal cord injury. Neural Regen. Res. 12, 702–713.
Silver, J., Schwab, M.E., Popovich, P.G., 2014. Central nervous system regenerative failure: role of oligodendrocytes, astrocytes, and microglia. Cold Spring Harb. Perspect. Biol. 7, a020602.
Spejo, A.B., Moon, L.D.F., 2018. An intriguing way to enhance rehabilitation of grasping in rats after spinal cord injury. Brain J. Neurol. 141, 1888–1899.
Stellwagen, D., Shatz, C.J., 2002. An instructive role for retinal waves in the development of retinogeniculate connectivity. Neuron 33, 357–367.
Tan, A.M., Chakrabarty, S., Kimura, H., Martin, J.H., 2012. Selective corticospinal tract injury in the rat induces primary afferent fiber sprouting in the spinal cord and hyperreflexia. J. Neurosci. 32, 12896–12908.
Tedeschi, A., Bradke, F., 2017. Spatial and temporal arrangement of neuronal intrinsic and extrinsic mechanisms controlling axon regeneration. Curr. Opin. Neurobiol. 42, 118–127.
Torres-Espin, A., Forero, J., Fenrich, K.K., Lucas-Osma, A.M., Krajacic, A., Schmidt, E., Vavrek, R., Raposo, P., Bennett, D.J., Popovich, P.G., Fouad, K., 2018. Eliciting inflammation enables successful rehabilitative training in chronic spinal cord injury. Brain J. Neurol. 141, 1946–1962.
Tremblay, M.E., Lowery, R.L., Majewska, A.K., 2010. Microglial interactions with synapses are modulated by visual experience. PLoS Biol. 8, e1000527.
Ueno, M., Nakamura, Y., Li, J., Gu, Z., Niehaus, J., Maezawa, M., Crone, S.A., Goulding, M., Baccei, M.L., Yoshida, Y., 2018. Corticospinal circuits from the sensory and motor cortices differentially regulate skilled movements through distinct spinal interneurons. Cell Rep. 23 (1286–1300), e1287.
Vallieres, N., Berard, J.L., David, S., Lacroix, S., 2006. Systemic injections of lipopolysaccharide accelerates myelin phagocytosis during Wallerian degeneration in the injured mouse spinal cord. Glia 53, 103–113.
Weidner, N., Ner, A., Salimi, N., Tuszynski, M.H., 2001. Spontaneous corticospinal axonal plasticity and functional recovery after adult central nervous system injury. Proc. Natl. Acad. Sci. U. S. A. 98, 3513–3518.
Williams, P., Jiang, Y.Q., Martin, J.H., 2017. Motor system plasticity after unilateral injury in the developing brain. Dev. Med. Child Neurol. 59, 1224–1229.
Wong-Riley, M.T., 1989. Cytochrome oxidase: an endogenous metabolic marker for neuronal activity. Trends Neurosci. 12, 94–101.
Yeung, M.S., Zdunek, S., Bergmann, O., Bernard, S., Salehpour, M., Alkass, K., Perl, S., Tisdale, J., Possnert, G., Brundin, L., Druid, H., Frisen, J., 2014. Dynamics of oligodendrocyte generation and myelination in the human brain. Cell 159, 766–774.
Zareen, N., Dodson, S., Armada, K., Awad, R., Sultana, N., Hara, E., Alexander, H., Martin, J.H., 2018. Stimulation-dependent remodeling of the corticospinal tract requires reactivation of growth-promoting developmental signaling pathways. Exp. Neurol. 307, 133–144.
Z'Graggen, W.J., Metz, G.A., Kartje, G.L., Thallmair, M., Schwab, M.E., 1998. Functional recovery and enhanced corticofugal plasticity after unilateral pyramidal tract lesion and blockade of myelin-associated neurite growth inhibitors in adult rats. J. Neurosci. 18, 4744–4757.